

Tremor burst and triggering processes in Cascadia after the 2022 Hunga Tonga-Hunga Ha'apai volcanic eruption

Sambit Sahoo^a, Batakrushna Senapati^a, Bhaskar Kundu^a, Yijian Zhou^b,
Abhijit Ghosh^b and Shuanggen Jin^{c,d}

^aDepartment of Earth and Atmospheric Sciences, NIT Rourkela, Rourkela, India; ^bDepartment of Earth and Planetary Sciences, University of California, Riverside, CA, USA; ^cSchool of Surveying and Land Information Engineering, Henan Polytechnic University, Jiaozuo, China; ^dShanghai Astronomical Observatory, Chinese Academy of Sciences, Shanghai, China

ABSTRACT

Episodic Tremors and Slip (ETS) are highly susceptible and sensitive to external stress perturbations. The tidal and remote triggering phenomena of tremors are well-documented globally, however, the significance of the delayed triggering mechanism remains elusive. In this paper, the possibilities of the tremor modulation by the Lamb waves induced from the Hunga Tonga-Hunga Ha'apai volcanic eruption (SW Pacific) on 15 January 2022 have been explored. The increasing activity of tremors after eruption has been explored at the study region of Cascadia subduction zone where such tremor do not correlate with tidal stress perturbations or remote triggering by far-off or near-by earthquakes. The increasing tremor activities are observed during the propagation of the Lamb wave cycles (L_1 , L_2 , L_3 , L_4) and more interestingly during inter-ETS period. From the seismic waveform analysis, we observe two coherent packets of teleseismic energy on 15 January 2022, which corresponds to arrival of surface and Lamb waves, respectively. The delayed triggering of tremors may be linked either with the teleseismic surface waves or Lamb waves from the volcanic explosion, or both. Although we cannot rule out coincidence, the delayed triggering by Lamb waves appears to be consistent with magnitude-dependent time delay and 2-D coupled pore pressure induced diffusion model.

ARTICLE HISTORY

Received 22 March 2024
Accepted 21 September 2024


KEYWORDS

Hunga Tonga-Hunga Ha'apai; Cascadia subduction zone; Lamb waves; delay triggering; pore pressure; non-volcanic tremors; teleseismic waves

1. Introduction

Low and very low-frequency earthquakes (LFEs and VLFEs), as well as tremors, can occur not only in volcanic regions but also in the deeper segments of active fault systems, such as convergent plate boundaries and transform faults. These tremor

CONTACT Bhaskar Kundu  rilbhaskar@gmail.com

 Supplemental data for this article can be accessed online at <https://doi.org/10.1080/19475705.2024.2409279>.

© 2024 The Author(s). Published by Informa UK Limited, trading as Taylor & Francis Group.

This is an Open Access article distributed under the terms of the Creative Commons Attribution-NonCommercial License (<http://creativecommons.org/licenses/by-nc/4.0/>), which permits unrestricted non-commercial use, distribution, and reproduction in any medium, provided the original work is properly cited. The terms on which this article has been published allow the posting of the Accepted Manuscript in a repository by the author(s) or with their consent.

occurrences may persist for several days depending on the region and associated deformation source (Obara 2002; Rogers and Dragert 2003). The tremor occurrence can be repetitive or episodic in nature which are referred as episodic tremor and slip (ETS), and provide significant insights about the stress/frictional regime in the brittle-ductile transition zone (Ghosh et al. 2009, 2012, 2015; Peng and Gomberg, 2010; Shelly et al. 2011; Hutchison and Ghosh 2016, 2017, 2019; Li and Ghosh 2017; Chaudhuri and Ghosh 2022). The rheology of the converging plate separates the subducting oceanic crust with the fluid enriched brittle-ductile transition zone, which behaves as the slip zone and the brittle zone as the locked zone (Kao et al. 2006). The continuous stress transformation at the slip zones also provides an idea about the stress accumulations at the adjacent brittle locked segments, which appear to be the hosts of the great earthquakes during strain release (Kao et al. 2006, 2007, 2009; Wang et al. 2008). At the western coast of the United States, the Juan de Fuca plate converges beneath the North American plate below the Pacific Ocean, forming the Cascadia subduction zone extending from Northern California to the Northern Vancouver islands, that has considered to be one of the best instrumentally monitored region of ETS (Wech and Creager, 2011). In the Cascadia subduction zone, tremors and very low-frequency earthquakes are well documented (Wech and Creager, 2011; Ghosh et al. 2015; Hutchison and Ghosh 2016, 2019; Wu et al. 2019; Chaudhuri and Ghosh 2022). A large number of tremors occur during the episodic slip with a recurrence period of 10 to 19 months (Miller et al. 2002; Rogers and Dragert 2003; Brudzinski and Allen 2007; Rubinstein et al. 2007; Dragert et al. 2014).

Moreover, tremor activity appears to be highly sensitive to external stress perturbations such as tidal loading (Rubinstein et al. 2008; Lambert et al. 2009; Thomas et al. 2009; Hawthorne and Rubin 2010; 2012; Royer et al. 2015; Houston 2015), arrival of seismic waves from near/far-off earthquakes (Miyazawa and Mori 2005, 2006; Rubinstein et al. 2007; Shelly et al. 2011; Pollitz et al. 2012; Peng et al. 2015; Kundu et al. 2016), hydrological loading (Pollitz et al. 2013) and even low-barometric pressure during passages of typhoons (Liu et al. 2009; Hsu et al. 2015; Kundu, 2022). Dynamic triggering of tremors and/or small earthquakes instantaneous with the passage of seismic waves or delayed for several hours are well documented (e.g. Shelly et al. 2011; Peng et al. 2015; Mendoza et al. 2016; Li et al. 2019). Further, Small dynamic stress in the order of kPa is enough to trigger tremors or small earthquakes (Ghosh et al. 2009; Rubinstein et al. 2009; Peng et al. 2015 ; Sahoo, 2024;). The processes involving the triggering of tremors remain sensitive due to the presence of high fluid activity and low nucleation time requirements for the events and hence, can provide a proxy about the subsurface critical stress and frictional conditions (Shelly et al. 2006; Audet et al. 2009; Peng et al. 2015; Petrosino et al. 2018; Sahoo et al. 2021). However, the significance of these triggered events remains elusive, especially for the delayed triggering mechanism.

In this article, we have investigated the different possibilities of the triggering (or seismicity modulation) process of the specific set of tremors at the Cascadia subduction zone, constraining different datasets and models (Figure 1). The accelerated tremor occurrence at the study region have been analysed to occur in the non-periodic inter-ETS time period in the Cascadia subduction zone (i.e. the tremors

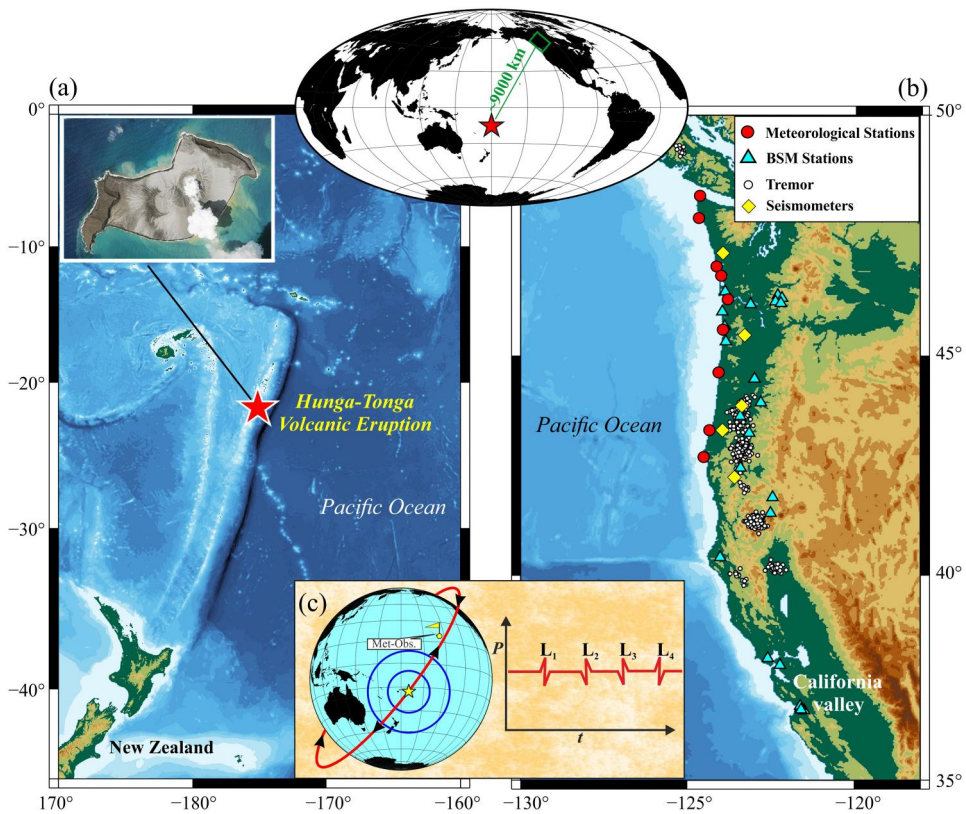


Figure 1. (a) Location of the 15th January, 2022 Hunga Tonga Hunga ha’pai volcanic eruption is marked by the red star. (b) Epicentral distribution of the tremors used in present study (white circles) at the Cascadia subduction zone for the period of 10th to 25th Jan, 2022. The red circles, cyan triangles and yellow diamonds represent the meteorological stations, borehole strainmeter stations (BSM) and seismometers, respectively, at the Coast of Cascadia subduction zone. (c) Schematic representation of the Lamb wave, which was induced due to the volcanic eruption, traveling around the globe several times. The upper inset shows the location of the volcano and Cascadia subduction zone and the distance travelled by the Lamb waves to reach the Cascadia subduction zone.

occurring in the usual quiescence between consecutive ETS period). We have applied some statistical methods to explore the possibility of triggering of the accelerated tremors by the various energy waves released from the massive volcanic eruption. Further, we have calculated tidal stress perturbations at the tremor occurrence zone and have examined teleseismic waves from the surrounding regions during the specific tremor occurrence period. The tremors are then correlated with the delay triggering characteristics by Lamb wave phases and/or teleseismic waves induced by the 2022 Hunga Tonga-Hunga Ha’apai volcanic eruption (or in short, Hunga Tonga eruption). Further, the delay triggering mechanisms are tried to be explained through the possible magnitude-dependent time delay, along with the 2-D coupled pore-pressure induced diffusion model.

2. January 15, 2022, Hunga Tonga volcano eruption and Lamb wave propagations

A large submarine volcanic eruption occurred on January 15, 2022, at Hunga Tonga-Hunga Ha'apai volcano, southern Pacific along the Tonga-Kermadec intra-oceanic arc (Figure 1). Two small, ~ 2 -km-long, uninhabited islands (i.e. Hunga Tonga and Hunga Ha'apai), rising to ~ 114 meters above sea level, currently represent the summit of the submarine volcano. They were connected by a new island (central cone) produced during the late 2014 to early 2015 eruption sequence and again got separated after this explosive eruption (Brenna et al. 2022). The Global Volcanism Program identified the eruption as starting at 04:15 UTC with a plume reaching 30 km in the atmosphere and 600 km in diameter. This volcanic eruption can be considered a 'once-in-a-century' event in the era of modern satellite observations due to the massive energy released from it and several first of its kind physical observations around the globe (D'Arcangelo et al. 2022, 2023; Lin et al. 2022; Matoza et al. 2022; Dalal et al. 2023). Numerous barometric arrays and ocean bottom pressure sensors around the globe captured Lamb waves and shock waves that rippled through the earth's atmosphere and there are reports of the event having been heard in New Zealand, Alaska and Yukon, Canada, Cascadia, etc. (D'Arcangelo et al. 2022, 2023; Lin et al. 2022; Matoza et al. 2022; Dalal et al. 2023). Although after Mt. Pinatubo (Philippines) volcanic eruption in 1991, long trains of infrasonic and acoustic-gravity waves were recorded by several ground-based stations in Japan and around the globe, Lamb waves were only documented during the Krakatau volcanic eruption in 1883 (Chimonas 1973; Kanamori and Mori 1992). Lamb waves propagated about ~ 9000 km horizontally and were reported in the different barometric sensors after 4 h of eruption in the Cascadia subduction zone (Figure 1). Lamb waves are a type of acoustic Rayleigh wave that propagates through solid plates along the mediating free surface and more explicitly, it is a type of boundary wave that behaves like an acoustic wave in the horizontal direction, maintaining hydrostatic equilibrium in the vertical direction. Further, teleseismic waves were also generated from the Hunga Tonga volcanic eruption (Poli and Shapiro 2022). Although the Lamb wave observations are limited but there have also been reports of change in far-field groundwater system induced by Lamb waves from the 2022 Hunga Tonga volcanic eruption (Zhang et al. 2024). Therefore, we believe, like teleseismic waves, the Lamb waves may have an impact on the fluid flow system which on the other hand can contribute to the triggering/modulation of the tremor activity, although such examples are lacking. Hence, the present scenario provides us with an exciting opportunity to explore the possible triggering (or modulation) of the tremor activity, explicitly during the inter-ETS period at the Cascadia subduction zone, after the 2022 Hunga Tonga volcanic eruption.

3. Data sets and models

In order to establish the possible tremor triggering/modulation process at the Cascadia subduction zone and the sensitivity of the tremors to the applicable stress perturbations, we have explored multiple datasets (e.g. tremor catalogue, barometric

pressure, borehole strainmeters, water level and seismic waveform data), as well as tidal stress derived from theoretical models that have been discussed below in the appropriate sections.

3.1. Tremor catalogue

In order to characterize the phenomena related to the triggering of the ETS sequence in central Cascadia, the tremor catalogue data from the Pacific Northwest Seismic Network (PNSN) has been used. The network has been operated and maintained by the University of Washington and the University of Oregon and archived in the public domain (see Data and Resources Section).

3.2. Barometric pressure

To characterize the different phases of Lamb waves (L_1 , L_2 , L_3 , L_4 , L_5 , L_6) of the Hunga Tonga volcanic eruption, we have explored barometric pressure data from various meteorological stations located on the coast of the Cascadia subduction zone (Figure 1b) and also followed the already reported literature (Lin et al. 2022; Dalal et al. 2023). These meteorological stations are operated by Centre for Operational Oceanographic Products and Services (CO-OPS) and controlled by the National Oceanographic and Atmospheric Administration (NOAA). Barometric data can be accessed and archived at NOAA (see Data and Resources Section). We use the standard sampling rate of 6 min of real-time series of barometric pressure data, in order to quantify the pressure changes in five to six consecutive days, induced by the Lamb wave oscillations after the 2022 Hunga Tonga volcanic eruption.

3.3. Borehole strain and water level data

The strain data used in this study has been archived from borehole strainmeter (BSM) networks, operated and maintained by the Geodetic Facility for the Advancement of Geosciences (GAGE) (Figure 1b), and available in the public domain from UNAVCO and IRIS (see Data and Resources Section). We use the standard sampling rate of 300 s of borehole strain data from B030, B031, B032, and B035 to characterize the arrival of Lamb waves phases (i.e. L_1 , L_2 , L_3 , L_4 , L_5 , L_6) in the location of tremor source at the Cascadia subduction zone. These time series data for the changes in the observed strain are filtered using a 10–100 min bandpass filter for a better representation. To correlate the water height with the tremor occurrence, we have used the water level time series from the La Push station (Figure 1b), archived by the National Oceanographic and Atmospheric Administration, NOAA (see Data and Resources Section).

3.4. Seismic data

To analyze the seismic waveforms generated from the 15 January 2022 Hunga Tonga volcanic eruption and its signature at the Cascadia coast, we have used data from five

broadband seismometers maintained by the Pacific Northwest Seismic Network (CORE, MINN, DRAN, LAIR and CAVE) which are publicly available. Using the datasets, we have captured the arrival of teleseismic waves from the 2022 Hunga Tonga volcanic eruption to the source zone of triggered tremor ~ 9000 km away at the Cascadia subduction zone.

3.5. Tidal model

We have used the SPOTL program (Agnew 1997, 2012) to estimate the stress exerted by tidal loading at a representative location at the middle of the Cascadia subduction zone (i.e. 43.5°N , -123.5°E). The tidal strains (i.e. extensional, shear strains, and volumetric strains) are calculated precisely from the corresponding positions of the Sun and Moon by assuming Green's functions from the Gutenberg-Bullen Earth model (Farrell 1972) and an elastic and spherical Earth model with satellite estimated Cartwright-Taylor constituent amplitudes with 2nd degree Love numbers as $h = 0.6114$, $k = 0.3040$, and $l = 0.0832$. During the estimation of tidal strains, different ocean tidal models were used, such as GOT4.7 global ocean tidal model (Ray 1999) and regional ocean tidal model produced by the Oregon State University (OSU) for the United States western coast (Egbert and Erofeeva 2002). We combined the loading from both models and used eight major short-period tidal constituents (K1, K2, M2, N2, O1, P1, Q1, and S2) to calculate the strains at the specific point accurately. Finally, to compute the tidal stress from the estimated strains, we have considered an elastic modulus of 30 GPa and a Poisson ratio of 0.25. The strains are rotated by using linear-elastic constitutive equations on the fault plane orientation (strike: 0° , dip: 22° , rake: 90°) for the estimation of the fault normal stress and fault parallel shear stress at the Cascadia subduction zone. The Coulomb failure stress is calculated considering the frictional coefficient as 0.3 (Sahoo et al. 2021).

4. Results and discussions

4.1. Triggering of tremors and possibilities

The sensitivity of tremors is always high for external stress perturbations for instantaneous as well as delayed modulations (Ghosh et al. 2009; Rubinstein et al. 2009; Peng et al. 2015). Increased tremor activity is largely controlled by the ongoing ETS events (Obara and Kato 2016) or they can also be modulated by major forces such as tidal loading (Thomas et al. 2009; 2012), seismic waves from remote earthquakes passing through the source fault (Gomberg 2010; Shelly et al. 2011; Kundu et al. 2016), or sometimes even by passages of typhoons and related phenomena producing low-barometric pressure (Liu et al. 2009; Kundu 2022). Therefore, we have tried to explore all possible aspects of modulations. First of all, we have plotted the cumulative number of tremors along the Cascadia subduction zone as a function of time for the periods 2015 to 2022 (Figure 2a). Three cycles of the ETS events with a recurrence interval of ~ 19 months in central Cascadia have been observed and marked in the Figure (Figure 2b). The tremors that occurred from 10th to 25th January 2022 (marked in red) are not associated with the observed major cycles of the ETS events,

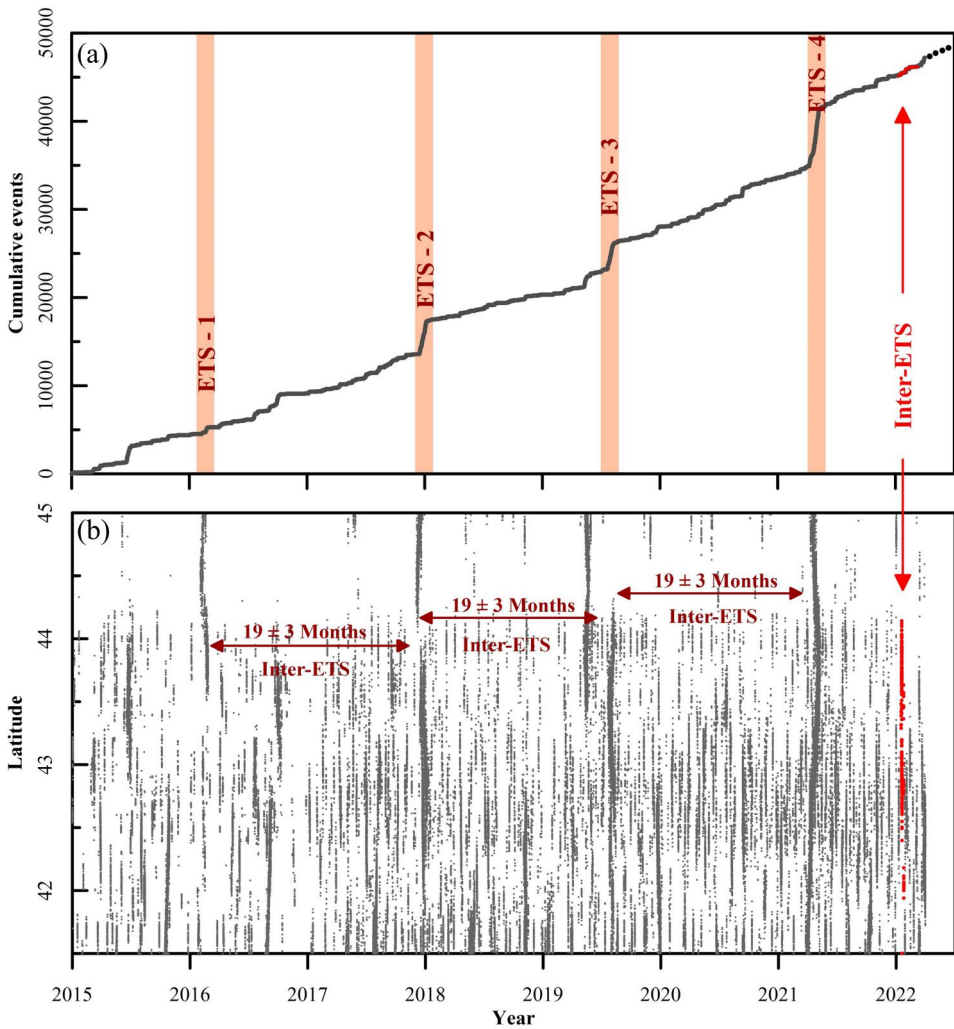


Figure 2. (a) Cumulative tremor number as a function of time. The various phase of the episodic slow slip and tremors (ETS) are marked by the orange strips. The red arrows represent the tremors analysed in the present study, that occurred between two ETS events. (b) Occurrence tremors time and latitudinal variation of tremor events for the periods of 2015 to 2022, shown with black dots. The red dots are tremors used in the present study for the periods of 10th to 25th January 2022. Note that tremors used in the present study occurred between two ETS periods (i.e. inter-ETS period).

which clearly show a steep increase in the cumulative no. of tremors in the upper panel (Figure 2a). Coming to the comparison with the time before and after the activity, we can also see other increased patches which are around ~ 4 -5 months before the event and ~ 1 -2 months after the events, which we believe cannot be related to the massive eruption event. In other words, the same tremor bursts we have tried to analyse here occur in the inter-ETS period. Hence, we can safely infer that it is not linked with any ongoing ETS events. Moreover, we have also gone through some statistical analysis to show that tremor activity is significantly higher during this time

period relative to its background activity, which are explained in the subsequent paragraph. This observation of heightened tremor activity during inter-ETS time motivated us to analyze the tremor modulation/triggering process in this area in detail. Here, we have explored the effects of various external forces (e.g. water level load, tidal load, teleseismic waves, Lamb waves, etc.) that possibly modulated/triggered tremors along the Cascadia subduction zone. We should point out that coincidence is also a possibility, and we have considered it as well.

In order to explore possible connection between the bursts of tremors and seismic/Lamb waves from the volcanic eruption, we have taken a statistical approach to test whether the tremors activity is significantly high compared to its background activity by applying the β statistics approach improvised from Aiken and Peng (2014):

$$\beta = \frac{N_a - N\left(\frac{T_a}{T}\right)}{\sqrt{\left(N\left(\frac{T_a}{T}\right)\right)\left(1 - \left(\frac{T_a}{T}\right)\right)}} \quad (1)$$

Where N_a are the events with possible triggering and N are total events, T_a is the time period of possible triggered tremors and T is the total time period. β values of ≥ 1.64 indicates statistically high activity at a triggered possibility confidence level of 90% whereas values ≥ 1.96 and ≥ 2.57 refer to 95% and 99% confidence levels of the possibility respectively (Matthews and Reasenberg 1988; Aiken and Peng 2014; Hill and Prejean 2015). Considering the scenario of possible triggering by external perturbations, we have taken the number of triggered events as 371 (N_a) (17th to 20th January) and the total number of events are 2772 (N) (1st December, 2021 to 31st January, 2022), where the time period for triggered events is around 70 h (T_a) in comparison to the total time period of events is around 1488 h (T) which were taken based on previous assumptions for analyzing the triggered nature of the tremor (Matthews and Reasenberg 1988; Aiken and Peng 2014; Hill and Prejean 2015). Therefore, the β value is found to be much larger than 2.57, which shows a more than 99% confidence level of the tremors being triggered in nature. This confirms that the tremors in the particular time period of study are triggered in nature.

4.2. Possibility of triggering by seismic waves from distant earthquakes

Seismic waves generated from large magnitude events are capable to trigger tremor activity in far-field and near-field regions from the source (Gomberg et al. 2004; Ghosh et al. 2009; Shelly et al. 2011; Pollitz et al. 2012; Hill and Prejean 2015; Peng et al. 2015; Kundu et al. 2016). Seismic waves can immediately trigger the tremors without any time delay, which can be explained by the Coulomb failure stress change model, when the external stresses generated from the seismic waves exceed the failure/triggering threshold on a critically stressed fault system (Hill 2012; Kundu et al. 2016). It can also possibly produce a delay in the triggering of tremor activity for some hours to a few days, which can be explained by the migration of fluid, non-linear friction, and aseismic deformation (Gomberg et al. 1997; Parsons 2005; Hill and Prejean 2015). In the present study, we have identified three large magnitude

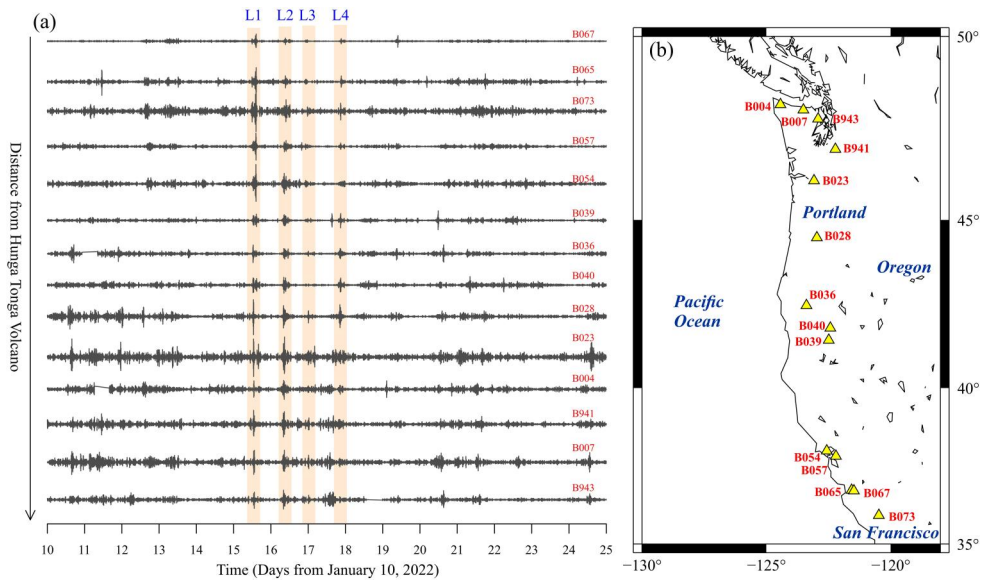


Figure 3. (a) Arrival of consecutive Lamb waves (L1, L2, L3, L4) at different borehole strainmeter stations with increase in distance from the Hunga Tonga volcano. (b) The borehole strainmeter array of the represented stations at the Cascadia region.

seismic events, based on their location and origin time, that may possibly influence this tremor burst in some way – a M6.2 event, located at the coast of Cascadia on 20 December 2021 and two M6.6 events in Alaska, on 11 January 2022 (Figure S1). The events with the largest possible energy occur well before the Hunga Tonga volcanic eruption, with the latest event taking place about a week before the tremor burst. Hence, it is unlikely that the seismic waves from distant earthquakes have greater impact than the Hunga Tonga eruption for potentially triggering the increased tremor activity in question.

4.3. Possible triggering of tremors by tidal loading

Importantly, tremors are highly sensitive to tidal loading and are well-documented with a high sensitivity around the worldwide subduction zones with prominent tremor activity (Lambert et al. 2009; Ide 2010; Gallego et al. 2013; Yabe et al. 2015). Therefore, we have analyzed the possibility of tidal triggering of the tremors in the Cascadia subduction zone for the period of 10th to 25th January 2022. The tremor catalogue was analysed for magnitude completeness (M_c) using the Gutenberg-Richter (GR) law using the reliable maximum likelihood approach and the M_c was found to be 1.0 (Aki, 1965) (Figure S2). We have explored the periodicity of the tremor (i.e. during that period) using power spectra analysis and observed that the tremor for the observed period does not show any significant tidal periodicity (Figure S3). Further, we have computed tidal stress at the source location of the tremor at the Cascadia and also correlated the tremors with the estimated Fault Normal Stress (FNS), Right-Lateral Shear Stress (RLSS), and Coulomb Failure Stress (CFS) from the total tidal loading (ocean + solid) (Figures 4a, 5a,b). For the quantification of the

degree of correlation between the tremors and the respective tidal stress, we have estimated the percentage of excess event numbers (N_{ex}) by following the approaches from Cochran et al. (2004), Thomas et al. (2012) and Sahoo et al. (2021). The N_{ex} numbers can be defined as the percentage of excess or deficit in events occurring during the particular time duration with respect to the expected number of events during the encouraging stress. It is expressed by the ratio percentage between the difference of the actual and expected number of events and the number of expected events and expressed as:

$$\text{Percentage of excess event}(N_{ex}) = \frac{N_{actual} - N_{expected}}{N_{expected}} \times 100 \quad (2)$$

where $N_{expected}$ is the expected number of events occurring under positive stress conditions, assuming there is a random distribution of the time of occurrence of events, and N_{actual} is the observed number of events occurring during the positive stress conditions. The phases (0° to 360°) of all seismic tremor events were calculated by the occurrence of the event in the particular angular position in the tidal stress cycle (peaks at 0° and 360° , trough at 180°) (Figure 5b). The phase values were then normalized to the phase values of the expected number of events after being grouped into 10° bins. The bins were represented as polar bar charts for respective tremor catalogue (Figures 4b, 5d). The grey bins of the specific radius in the bar chart represent the ratio of the observed number of events to the expected number of events ($N_{ex} + 1$) for that particular range of phase (Figures 4b, 5d).

From the statistical N_{ex} analysis and correlation analysis using polar bar charts, the results provide a significant correlation of the tremors with the negative tidal stress (low tides) during the observed period from 10th to 25th January 2022 (Figures 4b, 5d). The observation of the seismicity mostly occurring during the low tides (negative tidal stress) has become an interesting limitation for the tremor to be tidally triggered or triggered by increased water heights (or high tides) generated by the Hunga Tonga Eruption.

Although it has been suggested that tidal stresses at coastal regions are predominantly volumetric with very small deviatoric components, the N_{ex} value for the FNS is relatively insensitive to the choice of fault azimuth, while the N_{ex} value for the RLSS substantially changes according to the azimuth of stress estimation (Thomas et al. 2012). However, with predominantly linear segments with uniform fault azimuth associated with the Cascadia subduction reverse fault system, we can avoid such complexity in the present case. It also has been suggested that tremors at subduction reverse fault systems are modulated by high tides, as the loading from ocean tides is much greater at high tides, providing higher compressions to promote the slip (Cochran et al. 2004; Thomas et al. 2009, 2012; Royer et al. 2015).

From this analysis, it emerges that the correlation between tremors and FNS, RLSS, and CFS are not consistent with the expected results in a subduction zone environment (Figures 4b, 5d). Also, the tremors occurring at the low tides signify that the increased water wave heights (Figure 4c) due to the massive eruption are not the reasons for the initiation of the tremor occurrence. Thus the correlations with low tides and negative N_{ex} numbers of CFS suggest that the tremors are neither

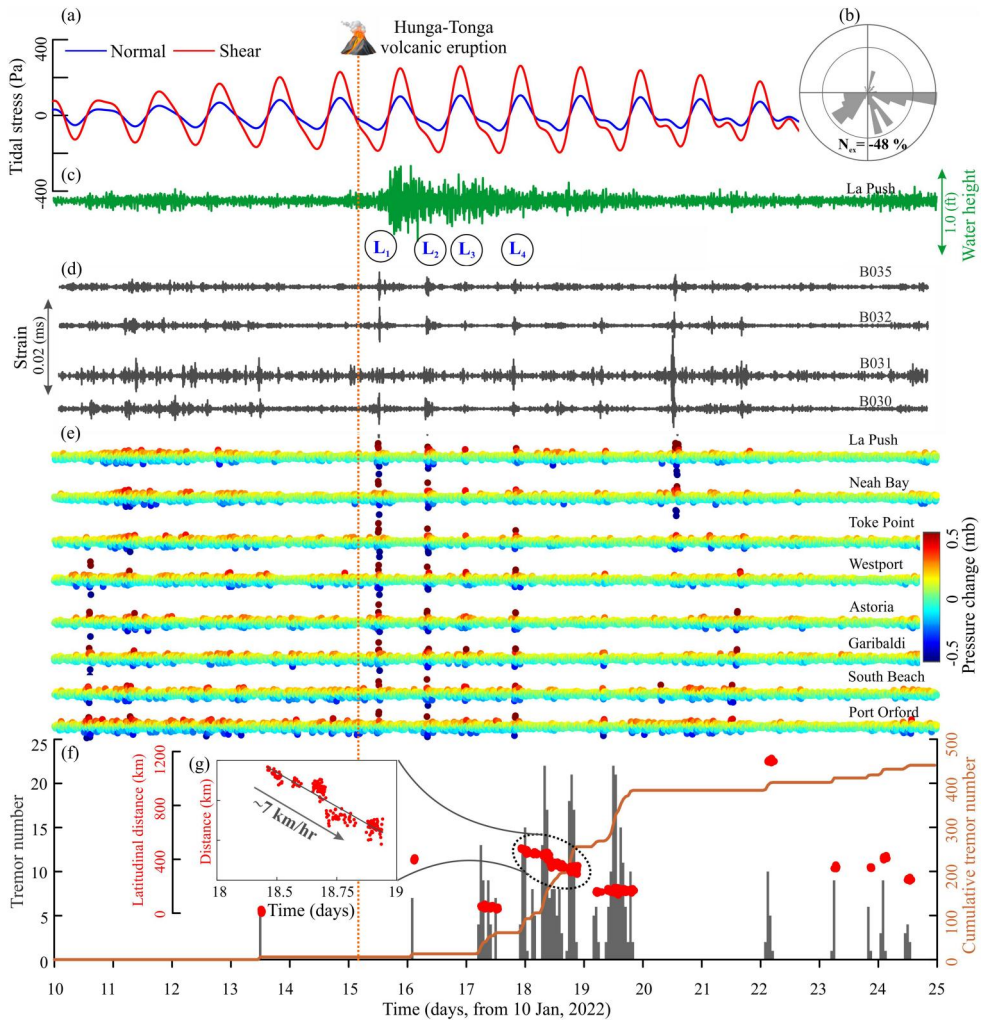
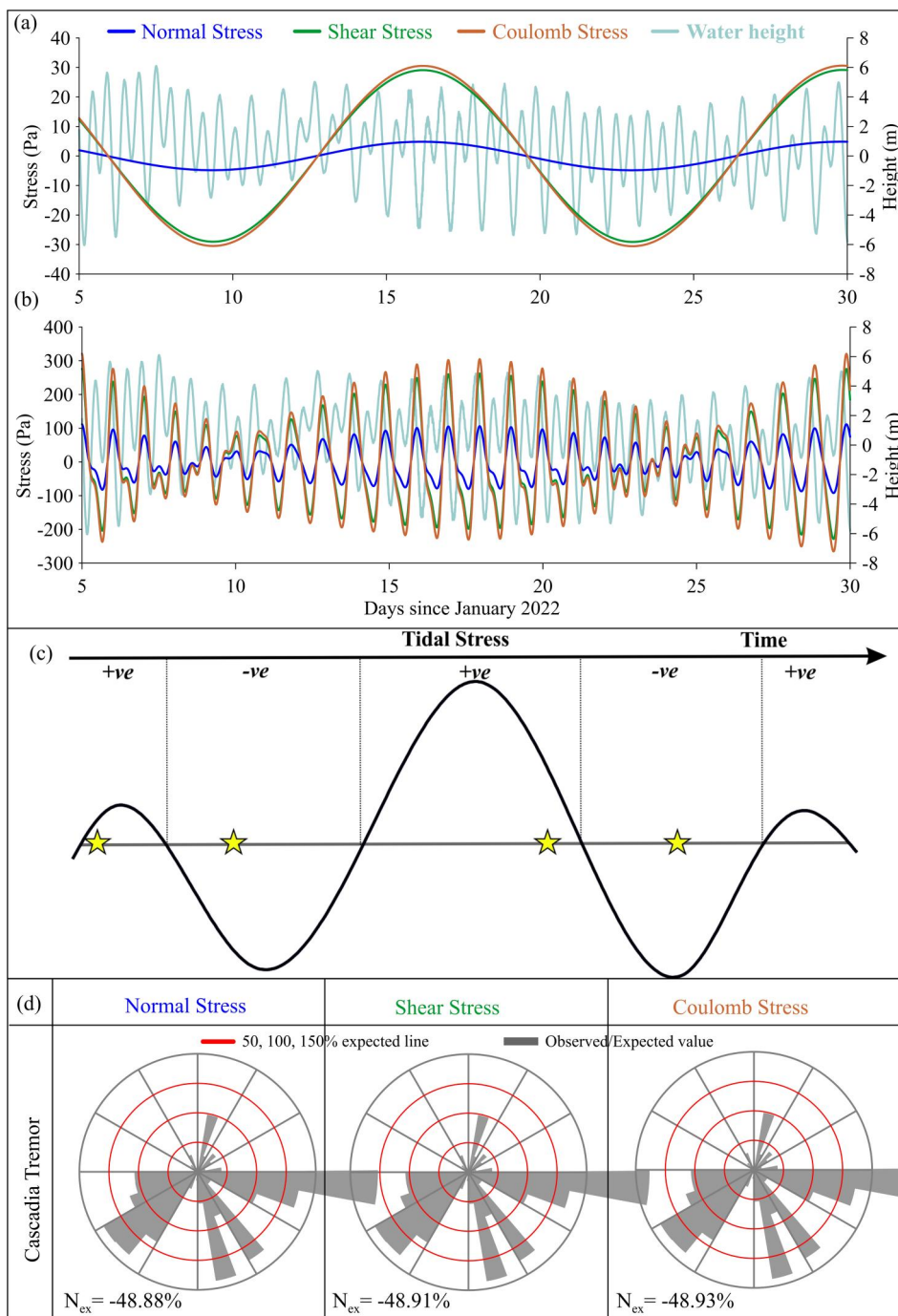


Figure 4. Time series analysis of tidal stress, water height, strain, barometric pressure and tremors, respectively. From top to bottom: (a) tidal stress variation (both normal and shear) resolved on the Cascadia subduction zone. (b) polar plot of the normal stress, where grey shaded areas indicate the ratio of observed to the expected number of events in each 10° phase bin (polar plots of shear and coulomb stress are shown in Figure 5). (c) The water levels variation at the La Push meteorological station is shown in green. (d) The variation of strain in the borehole strainmeters (BSM) are represented by grey lines. (e) The filtered time series of the barometric pressure are represented in coloured scale. (f) The hourly histogram and cumulative tremor number are represented by grey and orange colors, respectively. (g) Migration of tremors towards the southeast at a velocity ~ 7 km/hr. The orange dotted line shows the eruption of Tonga volcano. Note that the different phases of Lamb waves (L_1 , L_2 , L_3 , L_4) are observed in both barometric pressure data and BSM data.

correlated with the tidal loading or increased water heights (Figures 4c, 5d). Hence, we can also discard the possibility of tidal triggering phenomena as well as triggering from increased water levels for the tremors in the present case.



4.4. Possible triggering of tremors by Lamb wave from the 2022 Hunga Tonga eruption

Different phases of the Lamb wave (L_1, L_2, L_3, L_4) were generated from the massive submarine volcanic eruption on January 15th 2022 (04:14:45 UT), at the Hunga Tonga-Hunga Ha'apai volcano, along the Tonga-Kermadec intra-oceanic arc ~ 9000 km away from the tremor source from the Cascadia (Figure 1c) (D'Arcangelo et al. 2022; Lin et al. 2022; Dalal et al. 2023). The Lamb waves traveled multiple times around the globe (Figures 3a,b, 4 and Figures S4, S5; Dalal et al. 2023). The initial Lamb wave (L_1) was observed at several barometric stations along the Cascadia subduction zone after 4 h since the eruption (Figure 3a,b). Also, we have observed coherent Lamb waves across a wider region of the Cascadia subduction zone, which denotes the observation of the arrival of Lamb waves (L_1, L_2, L_3, L_4) ranging from 15th to 20th January 2022 for the available barometric and BSM datasets network (Figures S4–S7). Moreover, some signals of increasing strain and pressure values are also noticeable before and after the arrival of Lamb waves in both BSM and barometric stations for the remaining period of 10th January to 20th January and 20th January to 25th January 2022 (Figure 4d,e). These are the possible periodic variations due to the fortnightly tidal loading where the highest tides occur with a 14-day periodicity (Figure 5a). As the processed data from the strainmeter sensors are tidally corrected only for the daily variations of diurnal and semi-diurnal amplitudes, excluding the other monthly or fortnightly variations, the observed variations in the datasets explained above can be regarded as natural variations due to fortnightly tides. Therefore the observed fluctuations were related to disturbances generated by any particular event.

Hence, the respective time periods of variations in pressure and strain were also analyzed for the concurrent occurrence of any low-pressure weather fluctuation or storm activity at the Cascadia subduction zone which can also generate the observational fluctuations. However, we could not find any storm or coherent weather related activity in observations across the different weather stations and physical observatories at a wider region, where the fluctuations in the pressure and strain are observed. The occurrence of coherent fluctuations at such wider region without any



Figure 5. Representative tidal stress time series (total tidal stress = ocean + solid earth) along with observed water height at the Cascadia subduction zone presenting normal stress (NS), shear stress (SS), and Coulomb stress (CS) for the fortnightly tidal components (a) and all tidal components (b). Schematic diagram showing the variation of total tidal stress and the phase of seismic events associated with it. The peak and trough of the time series are assigned phase values of 0° and 180° , respectively. Dashed lines indicate the region of positive and negative tidal stress domains. Yellow stars represent hypothetical tremors, which correspond to either positive/negative stress fields (c). Polar phase plots and percent of the excess (N_{ex}) values of seismicity events (spanning from January 15th 2022 to January 21st 2022) by considering NS, SS, and CS components of total tidal stress. Gray shaded areas indicate the ratio of observed to the expected number of events in each 10-degree phase bin. Thin red lines are 50%, 100%, and 150% expected value contours. Note that in all cases of NS, SS and CFS the N_{ex} shows higher negative values, indicating the occurrence of events at high tides which does not relate with the mechanism of the events in the Cascadia region (d).

natural activity also confirms the fact that the fluctuations in the observation of pressure and strain parameters are completely due to the propagating Lamb waves.

During this period, the tectonic tremor activities increased at the Cascadia subduction zone from 15th to 21st January 2022. However, such heightened tremor activity is absent before the arrival of Lamb waves with some minor no. of events only on 13th January which was before the eruptions and much before the significantly higher events starting on 17th January (Figure 4f). Therefore, we have analyzed BSM data, barometric pressure data and they appear to coincide with the onset of high tremor activities. We observed that the increase of strain (compression) in the BSM data are synchronous with the arrival of Lamb waves, which indicates the possible Lamb wave induced oscillation and subsequent fluid migration in the source zone of tremors in the Cascadia subduction zone (Figure 4g). This speculation of Lamb wave induced fluid migration is also inspired by the fact that the Lamb waves can fluctuate the ground water systems which was also observed in the well water levels and strain-meters (Zhang et al. 2024). Interestingly, we have observed that the tremors activities increased 40-50 h after the arrival of L₁ phase of Lamb waves (i.e. 1st phase). Such time delay is consistent with the diffusion of the fluid flow which was initially triggered due to the propagating Lamb waves. We speculate that this process may trigger tremor considering that there have been previous reports of delayed dynamic triggering due to large seismic events (Delorey et al. 2015; Johnson and Bürgmann et al., 2015). This idea of a delayed triggering of the tremors due to the fluid movements from the effect of Lamb waves has been further discussed in the respective section for possible mechanism related to delayed triggering of tremors.

4.5. Possible triggering of tremors by teleseismic waves from the 2022, Hunga Tonga volcano eruption

Dynamic triggering of the tremors by teleseismic energy radiated from faraway earthquakes have also been reported at the Cascadia and other parts of the world with instantaneous effect (Ghosh et al. 2009; Gombert 2010; Kundu et al. 2016) as well as delayed relative to the passage of the teleseismic waves (Shelly et al. 2011). Long-period Love and Rayleigh waves are predominantly responsible for instantaneous dynamic triggering (Hill 2012). A few studies of body-wave-related triggering or modulation also have been reported at the Cascadia Subduction zone (Ghosh et al. 2009; Kundu et al. 2016).

The volcanic explosivity index (VEI) of the Hunga Tonga eruption is ~5-6 (Poli and Shapiro, 2022; Dalal et al. 2023), with a seismic estimate of an event in the range of 7-7.5 M_w (D'Arcangelo et al. 2023) which indicates that a large amount of energy was released on 15 January 2022, from the eruption. But the energy released to the atmosphere was much larger than a 7-7.5 M_w because, in comparison to the seismic energy where most of the energy is released in the lithosphere, in this case, maximum energy was released to the atmosphere (D'Arcangelo et al. 2022, 2023). Here, we have analyzed the available seismic data along the Cascadia margin focusing on southern Cascadia. We looked for teleseismic energy at lower frequencies (10 – 200 sec), and signal from local sources at 2-8 Hz, a typical frequency band for tectonic tremor. We

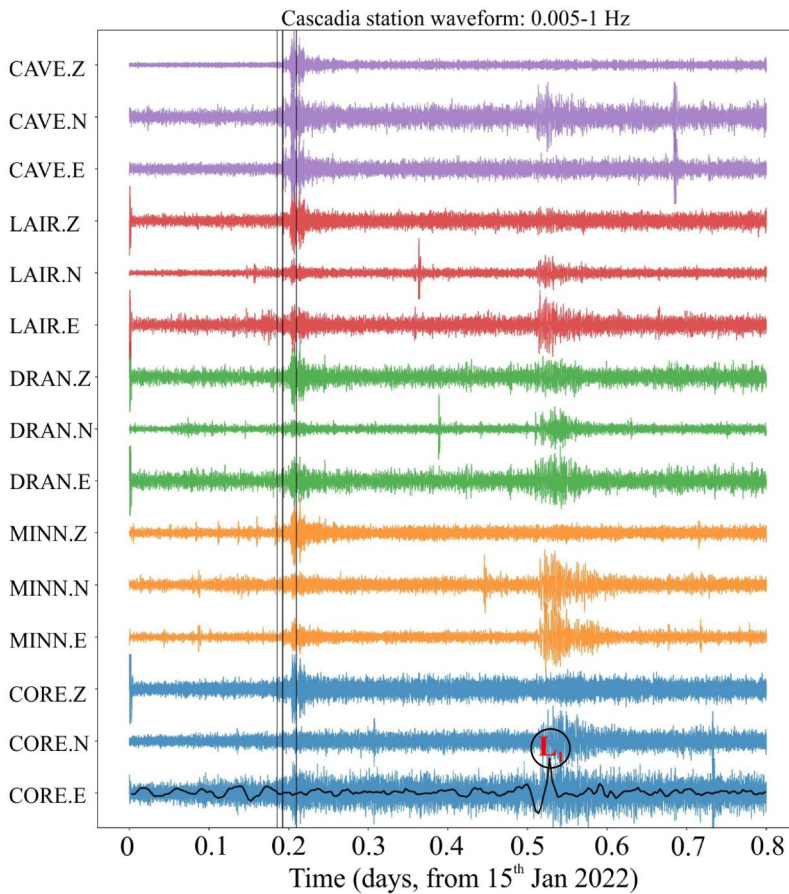


Figure 6. Seismic signals from broadband seismometers for the first 20 h on Jan 15, 2022. Seismic signals from broadband seismometers in Cascadia, filtered between 10 - 200s. Grey vertical lines show the theoretical arrival of teleseismic wave phases from Hunga Tonga eruption which is well documented (Poli and Shapiro, 2022). The borehole strain meter (BSM) signal from station B032 is represented in black horizontal lines and overlain with seismic signals for comparison. The first phase of Lamb wave arrival is marked as L_1 . Note that coherent packets of teleseismic energy observed at the time of 0.2 and 0.55 days.

found a clear teleseismic signal at the expected arrival time of surface, and atmospheric Lamb waves (L_1), which are shown in Figure 6. However, we do not find any obvious evidence of uncatalogued tremors during the passage of teleseismic waves. The fact that we observe long-period seismic waves coincident with the passage of atmospheric Lamb waves (L_1) indicates that Lamb waves are able to couple with solid earth. We speculate that two pulses of dynamic stress soon after one another, first teleseismic surface and then Lamb waves (L_1), may have triggered the fluid migration processes leading to the tremor episodes starting about 40 h later. Distinguishing and differentiating contributions from each of the wavetrains to the delayed triggering of tremor, however, are difficult to establish. We also note that instantaneous triggering by remote earthquakes is uncommon in southern Cascadia region (Rubinstein et al.

2009). Therefore, the absence of obvious tremors during the passage of teleseismic waves appears to be consistent with previous studies.

4.6. Mechanism of delay triggering

The possible delayed triggering of tremors and/or small earthquakes can be explained by several mechanisms, such as the surface wave generated from the earthquakes, volcanism, etc., which change the frictional properties of the fault zone and delay the nucleation process of earthquakes (Gomberg et al. 1997; Parsons 2005; Peng et al. 2011; Mendoza et al. 2016). In fact, the delay can be observed due to an elastic disturbance at the fault zone which can also generate a cascading effect of the stress transfer due to fluid migrations (Delorey et al. 2015). For further supportive evidences, we have also observed the possible migration of the tremors may be due to migration of fluid movements (i.e. migrate southeast at a velocity of ~ 7 km/hr), that we speculate were triggered by the L_1 phase of Lamb waves (Figure 3a). This tremor migration velocity is similar to the previously reported migration velocity (i.e. 7–17 km/hr) (Houston et al. 2011; Obara et al. 2012). In fact, the observed tremor migration velocity is higher than the propagation velocity of Lamb waves (~ 0.3 km/s), which implies that although the tremor activity is initiated by Lamb waves, it grows and migrates in a self-sustained manner. This may suggest a triggered transient slip event.

Surface waves can oscillate the deformation of a fault zone and break the previously existing path for fluid-flow into the fault zones. As a result, all invading fluids pass through the newly opened path into the fault zone and reduce the normal stress by increasing the pore fluid pressure (Parsons et al. 2017). This can be explained by the Coulomb failure stress change as $CFS = \tau - \mu(\sigma - p)$, where τ is the shear stress, μ is the friction coefficient of fault, σ is the normal stress and p is the pore fluid pressure. The migration of fluid into the fault zone reportedly takes hours or days to reduce the strength of the fault (Pollitz et al. 2012; Johnson et al. 2015; Johnson and Bürgmann 2016).

Thus, the time required to meet the failure conditions of the fault can potentially explain the delayed triggering of tremors. The seismic moment of the tremors is directly proportional to the rupture area of the fault zone, which can be expressed as $2L_c \approx \sqrt[3]{10^{-9} \times M_0}$, where $2L_c$ is the critical nucleation dimension of an earthquake and M_0 is the seismic moment (Ohnaka 2000). For a tremor to be induced by fluid pressure, the minimum fluid transit distance or the critical nucleation dimension ($2L_c$) of a fault zone should not be close (Parsons et al. 2017). Here, we have calculated the $2L_c$ of the individual tremor from the Cascadia subduction zone using the above governing equation and plotted against the time, considering the arrival time of the L_1 phase lamb wave as origin time (Figure 7a). We have calculated the diffusivity of the fault zone using the expression $D = \frac{r^2}{c^2 t}$ (Malagnini et al. 2012), where D is the diffusivity of the fault zone, c is a constant, distance from the source is presented as r , and t is the time. From this analysis, we observed that all the possibly triggered tremors in this study are in the diffusivity range of 10^{-4} to 10^{-6} m/s² (Figure 7b), which is consistent with the previously estimated diffusivity range of the fault zone

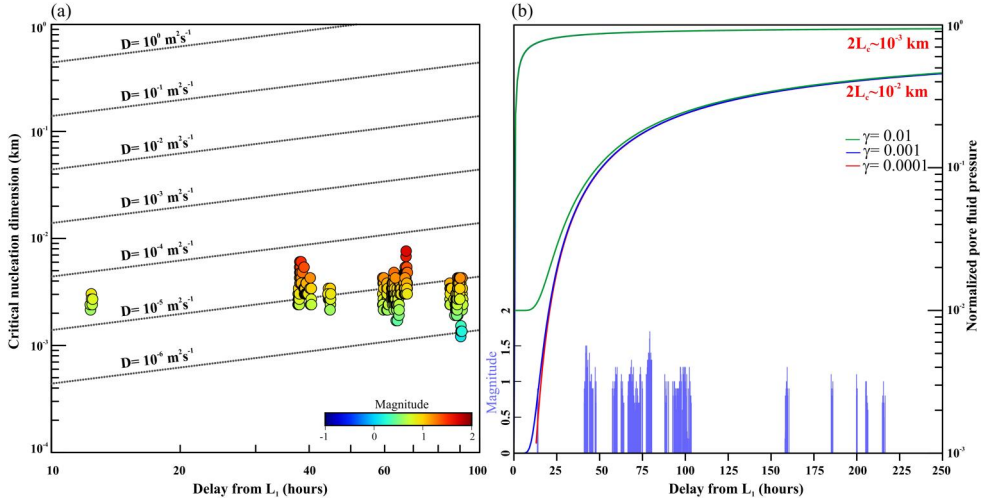


Figure 7. (a) Tremor occurrence times from the arrival of L₁ phase of Lamb waves plotted against their critical nucleation dimensions. The dotted lines represent the different crustal diffusivity. (b) 2-D coupled pore pressure-induced diffusion model. The normalized pore fluid pressure (P/P_0) calculated by considering ‘ r ’ as the critical nucleation dimension of the fault (i.e. 10^{-2} and 10^{-3} km) and D as 10^{-4} m/s² with varying γ as 0.01, 0.001 and 0.0001 respectively. Note that there is a 40-50 h’ phase delay between the L₁ phase of Lamb waves and tremor occurrence.

(Shapiro et al. 2006; Bourouis and Cornet, 2009; Tanikawa et al. 2014). This observed diffusivity of the fault zone is also consistent with the time versus critical nucleation dimension graph representing the delay observed, which also depends upon the magnitude of the event (Ohnaka 2000; Parsons et al. 2017).

Further, we suggest that such time delay in triggering between the L₁ phase of Lamb waves and tremor occurrence in the Cascadia subduction zone, can be explained by 2-D coupled pore pressure induced diffusion model (Mulargia and Bizzarri 2014). The coupled drained and undrained poroelastic pressure expressed as:

$$P(r, t) = \left. \begin{aligned} &\gamma P_0 \operatorname{erf}\left(\frac{r}{2\sqrt{Dt}}\right) + P_0 \operatorname{erf}\left(\frac{r}{2\sqrt{Dt}}\right) \\ &\gamma = \frac{B(1 + \vartheta)}{3(1 - \vartheta)} \end{aligned} \right\} \quad (3)$$

where P_0 is the initial fluid pressure, B is the Skempton’s coefficient, and ϑ is the Poisson’s ratio. For estimating the normalized pore fluid pressure (P/P_0), we have considered ‘ r ’ as the critical nucleation dimension of the fault (i.e. 10^{-2} and 10^{-3} km) and D as 10^{-4} m/s² with varying γ as 0.01, 0.001 and 0.0001 respectively. We find that normalized pore fluid pressure (P/P_0) is higher and becomes constant after the passage of 40-50 h with respect to the arrival time of the initial L₁ phase of Lamb waves (Figure 7b). The phase delay between the L₁ phase of Lamb waves and tremor occurrence is directly proportional to the critical nucleation dimension of the fault (Figure 7b). Hence, the observed phase delay between the L₁ phase of Lamb waves and tremor occurrence in the Cascadia subduction zone is consistent with the 2-D coupled pore pressure induced diffusion model.

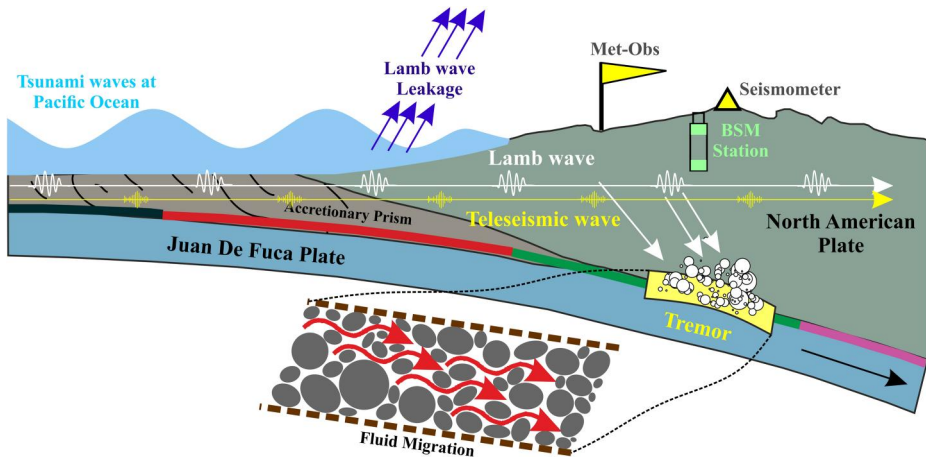


Figure 8. Schematic representation of the Cascadia tremor zone and Lamb/teleseismic waves propagation. The Lamb/teleseismic waves generated from the Tonga volcanic eruption propagated horizontally in the earth's surface. It disturbed the friction properties of the fault zone and generated new cracks and fractures for fluid migration. The fluid migrated through these newly opened cracks and fractures to the fault zone, reduced the fault strength, and triggered the tremors.

5. Conclusions

Based on this comprehensive analysis, we have proposed the following hypotheses related to the tremor burst and triggering activity which has also been schematically represented (Figure 8):

- Increasing intra-ETS tremor activities are observed in the Cascadia subduction zone during the propagation of the Hunga Tonga-Hunga Ha'apai volcanic eruption induced Lamb wave cycles (L1, L2, L3, L4).
- The tremor activity does not correlate with tidal stress perturbations or remote triggering by far-off or near-by earthquakes; however, it exhibits time lags of ~40-50 hours with the L1 phase of the Lamb wave.
- This time delay between the tremors bursts, and the different phases of Lamb waves appear to be consistent with magnitude-dependent time delay and 2-D coupled pore pressure induced diffusion model.

It should be also noted that distinguishing and differentiating contributions from different types of waves for this possible delayed triggering of tremors is difficult to establish. Also, we acknowledge that it is not possible to rule out that these tremor bursts can also be a coincidence. Although it seems unlikely considering the analyses presented.

Acknowledgments

We also thank Roland Bürgmann for discussions of the results, which significantly improved the quality of this work. BS has been supported by the NITR research fellowship. We thank the Committee of Research Senate grant from University of California, Riverside, for supporting this study. We would also like to thank Dr. Ramesh Singh, Editor in Chief, the Associate

Editor, and two anonymous reviewers for their constructive comments and suggestions, which significantly improved the quality of the work.

Disclosure statement

The authors declare no known competing financial interests or personal relationships that could have appeared to influence the work reported in this article.

Funding

This work was supported by the National Natural Science Foundation of China (NSFC) Project (Grant No. 12073012). SS was supported by the CSIR-UGC fellowship.

Data availability statement

Barometric arrays and ocean bottom pressure sensors around the globe captured Lamb waves and shock waves that rippled through the earth's atmosphere can be found at <https://nctr.pmel.noaa.gov/tonga20220115/> (last accessed April 26, 2022). The sound generated from the Hunga-Tonga Volcano heard in New Zealand, Alaska and Yukon, Canada, Cascadia etc. https://en.wikipedia.org/wiki/2022_Hunga_Tonga_eruption_and_tsunami (last accessed April 26, 2022). Information about Lamb waves and propagation (<https://www.eri.u-tokyo.ac.jp/en/news/4824/>) (last accessed April 26, 2022). The tremors data is archived from Pacific Northwest Seismic Network operated and maintained by the University of Washington and the University of Oregon and archived at <https://pnsn.org/tremor> (last accessed April 26, 2022). The barometric pressure data and water level data archive from National Oceanic and Atmospheric Administration, NOAA, <https://tidesandcurrents.noaa.gov/> (last accessed April 26, 2022). The borehole strainmeter (BSM) data are available from UNAVCO (<https://www.unavco.org/data/strain-seismic/bsm-data/bsm-data.htmlv>) (last accessed April 26, 2022). The Broadband seismogram data is maintained by the Pacific Northwest Seismic Network and archived at <https://pnsn.org/>. Plots were made using the Generic Mapping Tool, GMT, version 6.3.0 (www.soest.hawaii.edu/gmt/; Wessel et al. 2019) and Grapher, Version 10, Grapher™ from Golden Software, LLC (www.goldensoftware.com). All data used for the analysis are from public domains and can be downloaded from the provided links. The electronic supplement is attached with the supplementary figures (see the electronic supplement to this article).

References

- Agnew D. 2012. SPOTL: some programs for ocean-tide loading (SIO Technical Report). Scripps Instit of Oceanogr. University of California. <https://escholarship.org/uc/item/954322pg>.
- Agnew DC. 1997. NLOADF: a program for computing ocean-tide loading. *J Geophys Res.* 102(B3):5109–5110. doi: [10.1029/96JB03458](https://doi.org/10.1029/96JB03458).
- Aiken C, Peng Z. 2014. Dynamic triggering of microearthquakes in three geothermal/volcanic regions of California. *JGR Solid Earth.* 119(9):6992–7009. doi: [10.1002/2014JB011218](https://doi.org/10.1002/2014JB011218).
- Aki K. 1965. Maximum likelihood estimate of b in the formula $\log N = a - bM$ and its confidence limits. *Bull Earthquake Res Inst Tokyo Univ.* 43:237–239.
- Audet P, Bostock MG, Christensen NI, Peacock SM. 2009. Seismic evidence for overpressured subducted oceanic crust and megathrust fault sealing. *Nature.* 457(7225):76–78. doi: [10.1038/nature07650](https://doi.org/10.1038/nature07650).

- Bourouis S, Cornet FH. 2009. Microseismic activity and fluid fault interactions: some results from the Corinth Rift Laboratory (CRL), Greece. *Geophys J Int.* 178(1):561–580. doi: [10.1111/j.1365-246X.2009.04148.x](https://doi.org/10.1111/j.1365-246X.2009.04148.x).
- Brenna M, Cronin SJ, Smith IEM, Pontesilli A, Tost M, Barker S, Tonga'onevai S, Kula T, Vaiomounga R., 2022. Post-caldera volcanism reveals shallow priming of an intra-ocean arc andesitic caldera: hunga volcano, Tonga, SW Pacific. *Lithos.* 412–413:106614. doi: [10.1016/j.lithos.2022.106614](https://doi.org/10.1016/j.lithos.2022.106614).
- Brudzinski MR, Allen RM. 2007. Segmentation in episodic tremor and slip all along Cascadia. *Geol.* 35(10):907. doi: [10.1130/G23740A.1](https://doi.org/10.1130/G23740A.1).
- Chaudhuri K, Ghosh A. 2022. Widespread very low frequency earthquakes (VLFs) activity offshore cascadia. *Geophys Res Lett.* 49:13. doi: [10.1029/2022GL097962](https://doi.org/10.1029/2022GL097962).
- Chimonas G. 1973. Lamb waves generated by the 1970 solar eclipse. *Planet. Space Sci.* 21(11): 1843–1854. doi: [10.1016/0032-0633\(73\)90115-3](https://doi.org/10.1016/0032-0633(73)90115-3).
- Cochran ES, Vidale JE, Tanaka S. 2004. Earth tides can trigger shallow thrust fault earthquakes. *Science.* 306(5699):1164–1166. doi: [10.1126/science.1103961](https://doi.org/10.1126/science.1103961).
- D'Arcangelo S, Bonforte A, De Santis A, Maugeri SR, Perrone L, Soldani M, Arena G, Brogi F, Calcara M, Campuzano SA, et al. 2022. A multi-parametric and multi-layer study to investigate the largest 2022 hunga tonga–hunga ha'apai eruptions. *Remote Sens.* 14(15):3649. doi: [10.3390/rs14153649](https://doi.org/10.3390/rs14153649).
- D'Arcangelo S, Regi M, De Santis A, Perrone L, Cianchini G, Soldani M, Piscini A, Fidani C, Sabbagh D, Lepidi S, et al. 2023. A multiparametric-multilayer comparison of the preparation phase of two geophysical events in the TongaKermadec subduction zone: the 2019 M7.2 Kermadec earthquake and 2022 Hunga Ha'apai eruption. *Front Earth Sci.* 11:1267411. doi: [10.3389/feart.2023.1267411](https://doi.org/10.3389/feart.2023.1267411).
- Dalal P, Kundu B, Panda J, Jin S. 2023. Atmospheric Lamb wave pulse and volcanic explosivity index following the 2022 Hunga Tonga (South Pacific) eruption. *Front Earth Sci.* 10:931545. doi: [10.3389/feart.2022.931545](https://doi.org/10.3389/feart.2022.931545).
- Delorey AA, Chao K, Obara K, Johnson PA. 2015. Cascading elastic perturbation in Japan due to the 2012 M w 8.6 Indian Ocean earthquake. *Sci Adv.* 1(9):e1500468. doi: [10.1126/sciadv.1500468](https://doi.org/10.1126/sciadv.1500468).
- Dragert H, Wang K, Rogers G. 2014. Geodetic and seismic signatures of episodic tremor and slip in the northern Cascadia subduction zone. *Earth Planet Sp.* 56(12):1143–1150. doi: [10.1186/BF03353333](https://doi.org/10.1186/BF03353333).
- Egbert GD, Erofeeva SY. 2002. Efficient inverse modeling of barotropic ocean tides. *J Atmos Oceanic Technol.* 19(2):183–204. doi: [10.1175/1520-0426\(2002\)019<0183:EIMOBO>2.0.CO;2](https://doi.org/10.1175/1520-0426(2002)019<0183:EIMOBO>2.0.CO;2).
- Farrell WE. 1972. Deformation of the Earth by surface loads. *Rev. Geophys.* 10(3):761–797. doi: [10.1029/RG010i003p00761](https://doi.org/10.1029/RG010i003p00761).
- Gallego A, Russo RM, Comte D, Mocanu V, Murdie RE, VanDecar JC. 2013. Tidal modulation of continuous nonvolcanic seismic tremor in the Chile triple junction region. *Geochem Geophys Geosyst.* 14(4):851–863. doi: [10.1002/ggge.20091](https://doi.org/10.1002/ggge.20091).
- Ghosh A, Huesca-Pérez E, Brodsky E, Ito Y. 2015. Very low frequency earthquakes in Cascadia migrate with tremor. *Geophys Res Lett.* 42(9):3228–3232. doi: [10.1002/2015GL063286](https://doi.org/10.1002/2015GL063286).
- Ghosh A, Vidale JE, Creager KC. 2012. Tremor asperities in the transition zone control evolution of slow earthquakes. *J Geophys Res.* 117(B10):10301. doi: [10.1029/2012JB009249](https://doi.org/10.1029/2012JB009249).
- Ghosh A, Vidale JE, Peng Z, Creager KC, Houston H. 2009. Complex nonvolcanic tremor near Parkfield, California, triggered by the great 2004 Sumatra earthquake. *J Geophys Res.* 114(B12):B00A15. doi: [10.1029/2008JB006062](https://doi.org/10.1029/2008JB006062).
- Ghosh A, Vidale JE, Sweet JR, Creager KC, Wech AG. 2009. Tremor patches in Cascadia revealed by seismic array analysis. *Geophys Res Lett.* 36:17. doi: [10.1029/2009GL039080](https://doi.org/10.1029/2009GL039080).
- Gomberg J. 2010. Lessons from (triggered) tremor. *J Geophys Res.* 115(B10):B10302. doi: [10.1029/2009JB007011](https://doi.org/10.1029/2009JB007011).

- Gomberg J, Blanpied ML, Beeler NM. 1997. Transient triggering of near and distant earthquakes. *Bull Seismol Soc Am.* 87(2):294–309. doi: [10.1785/BSSA0870020294](https://doi.org/10.1785/BSSA0870020294).
- Gomberg J, Bodin P, Larson K, Dragert H. 2004. Earthquake nucleation by transient deformations caused by the $M=7.9$ Denali, Alaska, earthquake. *Nature.* 427(6975):621–624. doi: [10.1038/nature02335](https://doi.org/10.1038/nature02335).
- Hawthorne JC, Rubin AM. 2010. Tidal modulation of slow slip in Cascadia. *J Geophys Res.* 115(B9):B09406. doi: [10.1029/2010JB007502](https://doi.org/10.1029/2010JB007502).
- Hill DP, Prejean SG. 2015. 4.11 - Dynamic triggering. *Treatise on geophysics*. 2nd ed. USGS Pubs. Elsevier; p. 273–304. doi: [10.1016/B978-0-444-53802-4.00078-6](https://doi.org/10.1016/B978-0-444-53802-4.00078-6).
- Hill DP. 2012. Surface-wave potential for triggering tectonic (Nonvolcanic) tremor-corrected. *Bull Seismol Soc Am.* 102(6):2337–2355. doi: [10.1785/0120120086](https://doi.org/10.1785/0120120086).
- Houston H. 2015. Low friction and fault weakening revealed by rising sensitivity of tremor to tidal stress. *Nature Geosci.* 8(5):409–415. doi: [10.1038/ngeo2419](https://doi.org/10.1038/ngeo2419).
- Houston H, Delbridge BG, Wech AG, Creager KC. 2011. Rapid tremor reversals in Cascadia generated by a weakened plate interface. *Nature Geosci.* 4(6):404–409. doi: [10.1038/ngeo1157](https://doi.org/10.1038/ngeo1157).
- Hsu Y, Chang Y, Liu C, Lee H, Linde AT, Sacks SI, Kitagawa G, Chen Y. 2015. Revisiting borehole strain, typhoons, and slow earthquakes using quantitative estimates of precipitation-induced strain changes. *JGR Solid Earth.* 120(6):4556–4571. doi: [10.1002/2014JB011807](https://doi.org/10.1002/2014JB011807).
- Hutchison AA, Ghosh A. 2016. Very low frequency earthquakes spatiotemporally asynchronous with strong tremor during the 2014 episodic tremor and slip event in Cascadia. *Geophys Res Lett.* 43(13):6876–6882. doi: [10.1002/2016GL069750](https://doi.org/10.1002/2016GL069750).
- Hutchison AA, Ghosh A. 2017. Ambient tectonic tremor in the san jacinto fault, near the anza gap, detected by multiple mini seismic arrays. *Bull Seismol Soc Am.* 107(5):1985–1993. doi: [10.1785/0120160385](https://doi.org/10.1785/0120160385).
- Hutchison AA, Ghosh A. 2019. Repeating VLFes during ETS events in cascadia track slow slip and continue throughout inter-ETS period. *JGR Solid Earth.* 124(1):554–565. doi: [10.1029/2018JB016138](https://doi.org/10.1029/2018JB016138).
- Ide S. 2010. Striations, duration, migration and tidal response in deep tremor. *Nature.* 466(7304):356–359. doi: [10.1038/nature09251](https://doi.org/10.1038/nature09251).
- Ide S. 2012. Variety and spatial heterogeneity of tectonic tremor worldwide. *J Geophys Res.* 117:B3. doi: [10.1029/2011JB008840](https://doi.org/10.1029/2011JB008840).
- Johnson CW, Bürgmann R, Pollitz FF. 2015. Rare dynamic triggering of remote $M \geq 5.5$ earthquakes from global catalog analysis. *JGR Solid Earth.* 120(3):1748–1761. doi: [10.1002/2014JB011788](https://doi.org/10.1002/2014JB011788).
- Johnson CW, Bürgmann R. 2016. Delayed dynamic triggering: local seismicity leading up to three remote $M \geq 6$ aftershocks of the 11 April 2012 $M8.6$ Indian Ocean earthquake: delayed Triggering of Remote $M \geq 6$ Events. *JGR Solid Earth.* 121(1):134–151. doi: [10.1002/2015JB012243](https://doi.org/10.1002/2015JB012243).
- Kanamori H, Mori J. 1992. Harmonic excitation of mantle Rayleigh waves by the 1991 eruption of Mount Pinatubo, Philippines. *Geophys Res Lett.* 19(7):721–724. doi: [10.1029/92GL00258](https://doi.org/10.1029/92GL00258).
- Kao H, Shan S, Dragert H, Rogers G, Cassidy JF, Wang K, James TS, Ramachandran K. 2006. Spatial-temporal patterns of seismic tremors in northern Cascadia. *J Geophys Res.* 111:B3. doi: [10.1029/2005JB003727](https://doi.org/10.1029/2005JB003727).
- Kao H, Shan S-J, Dragert H, Rogers G. 2009. Northern Cascadia episodic tremor and slip: a decade of tremor observations from 1997 to 2007. *J Geophys Res.* 114(B11):3. doi: [10.1029/2008JB006046](https://doi.org/10.1029/2008JB006046).
- Kao H, Shan S-J, Rogers G, Dragert H. 2007. Migration characteristics of seismic tremors in the northern Cascadia margin. *Geophys. Res. Lett.* 34(3):L03304. doi: [10.1029/2006GL028430](https://doi.org/10.1029/2006GL028430).
- Kundu B, Ghosh A, Mendoza M, Bürgmann R, Gahalaut VK, Saikia D. 2016. Tectonic tremor on Vancouver Island, Cascadia, modulated by the body and surface waves of the $M_w 8.6$

- and 8.2, 2012 East Indian Ocean earthquakes: tectonic Tremor on Vancouver Island. *Geophys Res Lett.* 43(17):9009–9017. doi: [10.1002/2016GL069755](https://doi.org/10.1002/2016GL069755).
- Kundu B. 2022. Synchronous tremor modulation during the passage of 2012 super-typhoon Jelawat in Nankai trough: by chance or real consequence? *J Geol Soc India.* 98(2):169–172. doi: [10.1007/s12594-022-1953-x](https://doi.org/10.1007/s12594-022-1953-x).
- Lambert A, Kao H, Rogers G, Courtier N. 2009. Correlation of tremor activity with tidal stress in the northern Cascadia subduction zone. *J Geophys Res.* 114(B8):B00A08. doi: [10.1029/2008JB006038](https://doi.org/10.1029/2008JB006038).
- Li B, Ghosh A, Mendoza MM. 2019. Delayed and sustained remote triggering of small earthquakes in the san Jacinto fault region by the 2014 Mw 7.2 Papanoa, Mexico Earthquake. *Geophys Res Lett.* 46(21):11925–11933. doi: [10.1029/2019GL084604](https://doi.org/10.1029/2019GL084604).
- Li B, Ghosh A. 2017. Near-continuous tremor and low-frequency earthquake activities in the Alaska-Aleutian subduction zone revealed by a mini seismic array. *Geophys Res Lett.* 44(11):5427–5435. doi: [10.1002/2016GL072088](https://doi.org/10.1002/2016GL072088).
- Lin J, Rajesh PK, Lin CCH, Chou M, Liu J, Yue J, Hsiao T, Tsai H, Chao H, Kung M. 2022. Rapid conjugate appearance of the giant ionospheric lamb wave signatures in the northern hemisphere after hunga-tonga volcano eruptions. *Geophys Res Lett.* 49:e2022.
- Liu C, Linde AT, Sacks IS. 2009. Slow earthquakes triggered by typhoons. *Nature.* 459(7248): 833–836. doi: [10.1038/nature08042](https://doi.org/10.1038/nature08042).
- Malagnini L, Lucente FP, De Gori P, Akinci A, Munafo' I. 2012. Control of pore fluid pressure diffusion on fault failure mode: insights from the 2009 L'Aquila seismic sequence. *J Geophys Res.* 117:B5. doi: [10.1029/2011JB008911](https://doi.org/10.1029/2011JB008911).
- Mallapaty S. 2022. How the Tonga eruption is helping space scientists understand Mars. *Nature.* doi: [10.1038/d41586-022-00137-z](https://doi.org/10.1038/d41586-022-00137-z).
- Matoza RS, Fee D, Assink JD, Iezzi AM, Green DN, Kim K, Toney L, Lecocq T, Krishnamoorthy S, Lalande J-M, et al. 2022. Atmospheric waves and global seismoacoustic observations of the January 2022 Hunga eruption, Tonga. *Science.* 377(6601):95–100., doi: [10.1126/science.abo7063](https://doi.org/10.1126/science.abo7063).
- Matthews MV, Reasenber PA. 1988. Statistical methods for investigating quiescence and other temporal seismicity patterns. *PAGEOPH.* 126(2-4):357–372. doi: [10.1007/BF00879003](https://doi.org/10.1007/BF00879003).
- Mendoza MM, Ghosh A, Rai SS. 2016. Dynamic triggering of small local earthquakes in the central Himalaya. *Geophys Res Lett.* 43(18):9581–9587. doi: [10.1002/2016GL069969](https://doi.org/10.1002/2016GL069969).
- Miller MM, Melbourne T, Johnson DJ, Sumner WQ. 2002. Periodic slow earthquakes from the Cascadia subduction zone. *Science.* 295(5564):2423–2423. doi: [10.1126/science.1071193](https://doi.org/10.1126/science.1071193).
- Miyazawa M, Mori J. 2005. Detection of triggered deep low-frequency events from the 2003 Tokachi-oki earthquake. *Geophys. Res. Lett.* 32(10):L10307. doi: [10.1029/2005GL022539](https://doi.org/10.1029/2005GL022539).
- Miyazawa M, Mori J. 2006. Evidence suggesting fluid flow beneath Japan due to periodic seismic triggering from the 2004 Sumatra-Andaman earthquake. *Geophys. Res. Lett.* 33(5): L05303. doi: [10.1029/2005GL025087](https://doi.org/10.1029/2005GL025087).
- Mulargia F, Bizzarri A. 2014. Anthropogenic triggering of large Earthquakes. *Sci Rep.* 4(1): 6100. doi: [10.1038/srep06100](https://doi.org/10.1038/srep06100).
- Obara K, Kato A. 2016. Connecting slow earthquakes to huge earthquakes. *Science.* 353(6296): 253–257. doi: [10.1126/science.aaf1512](https://doi.org/10.1126/science.aaf1512).
- Obara K. 2002. Nonvolcanic deep tremor associated with subduction in Southwest Japan. *Science.* 296(5573):1679–1681. doi: [10.1126/science.1070378](https://doi.org/10.1126/science.1070378).
- Obara K, Matsuzawa T, Tanaka S, Maeda T. 2012. Depth dependent mode of tremor migration beneath Kii Peninsula, Nankai subduction zone. *Geophys Res Lett.* 39(10). doi: [10.1029/2012GL051420](https://doi.org/10.1029/2012GL051420).
- Ohnaka M. 2000. A physical scaling relation between the size of an earthquake and its nucleation zone size. *Pure Appl Geophys.* 157(11):2259–2282. doi: [10.1007/PL00001084](https://doi.org/10.1007/PL00001084).
- Parsons T, Malagnini L, Akinci A. 2017. Nucleation speed limit on remote fluid-induced earthquakes. *Sci Adv.* 3(8):e1700660. doi: [10.1126/sciadv.1700660](https://doi.org/10.1126/sciadv.1700660).
- Parsons T. 2005. A hypothesis for delayed dynamic earthquake triggering. *Geophys. Res. Lett.* 32(4):n/a–n/a. doi: [10.1029/2004GL021811](https://doi.org/10.1029/2004GL021811).

- Peng Z, Shelly DR, Ellsworth WL. 2015. Delayed dynamic triggering of deep tremor along the Parkfield-Cholame section of the San Andreas Fault following the 2014 *M* 6.0 South Napa earthquake. *Geophys Res Lett.* 42(19):7916–7922. doi: [10.1002/2015GL065277](https://doi.org/10.1002/2015GL065277).
- Peng Z, Gomberg J. 2010. An integrated perspective of the continuum between earthquakes and slow-slip phenomena. *Nature Geosci.* 3(9):599–607. doi: [10.1038/ngeo940](https://doi.org/10.1038/ngeo940).
- Peng Z, Wu C, Aiken C. 2011. Delayed triggering of microearthquakes by multiple surface waves circling the Earth. *Geophys Res Lett.* 38(4):n/a–n/a. doi: [10.1029/2010GL046373](https://doi.org/10.1029/2010GL046373).
- Petrosino S, Cusano P, Madonia P. 2018. Tidal and hydrological periodicities of seismicity reveal new risk scenarios at Campi Flegrei caldera. *Sci Rep.* 8(1):13808. doi: [10.1038/s41598-018-31760-4](https://doi.org/10.1038/s41598-018-31760-4).
- Poli P, Shapiro NM. 2022. Rapid characterization of large volcanic eruptions: measuring the impulse of the Hunga Tonga Ha’apai Explosion From Teleseismic Waves. *Geophys Res Lett.* 49:8. doi: [10.1029/2022GL098123](https://doi.org/10.1029/2022GL098123).
- Pollitz FF, Stein RS, Sevilgen V, Bürgmann R. 2012. The Apr 11 2012 east Indian Ocean earthquake triggered large aftershocks worldwide. *Nature.* 490(7419):250–253. doi: [10.1038/nature11504](https://doi.org/10.1038/nature11504).
- Pollitz FF, Wech A, Kao H, Bürgmann R. 2013. Annual modulation of non-volcanic tremor in northern Cascadia. *JGR Solid Earth.* 118(5):2445–2459. doi: [10.1002/jgrb.50181](https://doi.org/10.1002/jgrb.50181).
- Ray RD. 1999. A global ocean tide model from TOPEX/POSEIDON altimetry: GOT99. 2. National Aeronautics and Space Administration, Goddard Space Flight Center.
- Rogers G, Dragert H. 2003. Episodic tremor and slip on the cascadia subduction zone: the chatter of silent slip. *Science.* 300(5627):1942–1943. doi: [10.1126/science.1084783](https://doi.org/10.1126/science.1084783).
- Royer AA, Thomas AM, Bostock MG. 2015. Tidal modulation and triggering of low-frequency earthquakes in northern Cascadia. *JGR Solid Earth.* 120(1):384–405. doi: [10.1002/2014JB011430](https://doi.org/10.1002/2014JB011430).
- Rubinstein JL, Gomberg J, Vidale JE, Wech AG, Kao H, Creager KC, Rogers G. 2009. Seismic wave triggering of nonvolcanic tremor, episodic tremor and slip, and earthquakes on Vancouver Island. *J Geophys Res.* 114(B2):B00A01. doi: [10.1029/2008JB005875](https://doi.org/10.1029/2008JB005875).
- Rubinstein JL, La Rocca M, Vidale JE, Creager KC, Wech AG. 2008. Tidal modulation of non-volcanic tremor. *Science.* 319(5860):186–189. doi: [10.1126/science.1150558](https://doi.org/10.1126/science.1150558).
- Rubinstein JL, Vidale JE, Gomberg J, Bodin P, Creager KC, Malone SD. 2007. Non-volcanic tremor driven by large transient shear stresses. *Nature.* 448(7153):579–582. doi: [10.1038/nature06017](https://doi.org/10.1038/nature06017).
- Sahoo S, Senapati B, Panda D, Tiwari DK, Santosh M, Kundu B. 2021. Tidal triggering of micro-seismicity associated with caldera dynamics in the Juan de Fuca ridge. *J Volcanol Geotherm Res.* 417:107319. doi: [10.1016/j.jvolgeores.2021.107319](https://doi.org/10.1016/j.jvolgeores.2021.107319).
- Sahoo S, Senapati B, Panda D, Jin S, Kundu B. 2024. Tidal triggering of seismic swarm associated with hydrothermal circulation at Blanco ridge transform fault zone, Northeast Pacific. *Phys. Earth Planet. Inter.* 356(107259). doi: [10.1016/j.pepi.2024.107259](https://doi.org/10.1016/j.pepi.2024.107259)
- Shapiro SA, Kummerow J, Dinske C, Asch G, Rothert E, Erzinger J, Kämpel H-J, Kind R. 2006. Fluid induced seismicity guided by a continental fault: injection experiment of 2004/2005 at the German Deep Drilling Site (KTB). *Geophys. Res. Lett.* 33(1). doi: [10.1029/2005GL024659](https://doi.org/10.1029/2005GL024659).
- Shelly DR, Beroza GC, Ide S, Nakamura S. 2006. Low-frequency earthquakes in Shikoku, Japan, and their relationship to episodic tremor and slip. *Nature.* 442(7099):188–191. doi: [10.1038/nature04931](https://doi.org/10.1038/nature04931).
- Shelly DR, Peng Z, Hill DP, Aiken C. 2011. Triggered creep as a possible mechanism for delayed dynamic triggering of tremor and earthquakes. *Nature Geosci.* 4(6):384–388. doi: [10.1038/ngeo1141](https://doi.org/10.1038/ngeo1141).
- Tanikawa W, Mukoyoshi H, Lin W, Hirose T, Tsutsumi A. 2014. Pressure dependence of fluid transport properties of shallow fault systems in the Nankai subduction zone. *Earth Planet Sp.* 66(1):90. doi: [10.1186/1880-5981-66-90](https://doi.org/10.1186/1880-5981-66-90).

- Thomas AM, Bürgmann R, Shelly DR, Beeler NM, Rudolph ML. 2012. Tidal triggering of low frequency earthquakes near Parkfield, California: implications for fault mechanics within the brittle-ductile transition. *J Geophys Res.* 117(B5):n/a–n/a. doi: [10.1029/2011JB009036](https://doi.org/10.1029/2011JB009036).
- Thomas AM, Nadeau RM, Bürgmann R. 2009. Tremor-tide correlations and near-lithostatic pore pressure on the deep San Andreas fault. *Nature.* 462(7276):1048–1051. doi: [10.1038/nature08654](https://doi.org/10.1038/nature08654).
- University of Oregon. 1990. Pacific northwest seismic network - university of Oregon [Data set]. *Int Federat Dig Seismog Netw.* doi: [10.7914/SN/UO](https://doi.org/10.7914/SN/UO).
- Wang K, Dragert H, Kao H, Roeloffs E. 2008. Characterizing an “uncharacteristic” ETS event in northern Cascadia. *Geophys Res Lett.* 35(15):L15303. doi: [10.1029/2008GL034415](https://doi.org/10.1029/2008GL034415).
- Wech AG, Creager KC. 2011. A continuum of stress, strength and slip in the Cascadia subduction zone. *Nature Geosci.* 4(9):624–628. doi: [10.1038/ngeo1215](https://doi.org/10.1038/ngeo1215).
- Wessel P, Luis JF, Uieda L, Scharroo R, Wobbe F, Smith WHF, Tian D. 2019. The generic mapping tools version 6. *Geochem Geophys Geosyst.* 20(11):5556–5564. doi: [10.1029/2019GC008515](https://doi.org/10.1029/2019GC008515).
- Wu B, Oglesby DD, Ghosh A, Li B. 2019. A dynamic rupture source model for very low-frequency earthquake signal without detectable nonvolcanic tremors. *Geophys Res Lett.* 46(21): 11934–11943. doi: [10.1029/2019GL084135](https://doi.org/10.1029/2019GL084135).
- Yabe S, Tanaka Y, Houston H, Ide S. 2015. Tidal sensitivity of tectonic tremors in Nankai and Cascadia subduction zones. *JGR Solid Earth.* 120(11):7587–7605. doi: [10.1002/2015JB012250](https://doi.org/10.1002/2015JB012250).
- Zhang X, Chen M, Zhong T, De Santis A, Han P. 2024. Far-field groundwater response to the Lamb waves from the 2022 Hunga-Tonga volcano eruption. *Geophys Res Lett.* 51(11): e2023GL107442. doi: [10.1029/2023GL107442](https://doi.org/10.1029/2023GL107442).